Asian Journal of Chemistry; Vol. 38, No. 2 (2026), 434-442
ASIAN JOURNAL OF CHEMISTRY
https://doi.org/10.14233/ajchem.2026.35023

Green Synthesis of ZnO Nanoparticles Mediated by *Eleutherine bulbosa*: Multifunctional Properties for Biomedical and Environmental Applications

S. MONICA[1], P.R. KAVITHA RANI[1,*], C. THAMARAI CHELVI[1] and S. HARI PRASAD[2]

[1]P.G. and Research Department of Chemistry, The Standard Fireworks Rajaratnam College for Women (Affiliated to Madurai Kamaraj University), Sivakasi-626123, India
[2]P.G. and Research Department of Chemistry, University College (Affiliated to Kerala University), Thiruvananthapuram-695034, India

*Corresponding author: E-mail: raghavkavitha@gmail.com

Received: 10 October 2025 *Accepted*: 7 January 2026 *Published online*: 31 January 2026 AJC-22261

In this work, zinc oxide nanoparticles (ZnO NPs) were prepared using an eco-friendly aqueous extract of *Eleutherine bulbosa* bulbs and were characterised by spectral and morphological techniques. The XRD confirmed sharp peaks with a crystallite size of 27.21 nm. Morphological studies showed flake-like structures in SEM and predominantly spherical particles in HR-TEM. TGA demonstrated good thermal stability with a weight loss from 96% to 65%. Functionally, the ZnO NPs exhibited strong antioxidant activity (IC_{50} = 44.15 µg/mL) and potent anticancer effects against human breast cancer cells (IC_{50} = 21.12 µg/mL). Photocatalytic activity was also significant, achieving 80% methylene blue degradation under UV light within 100 min.

Keywords: Green synthesis, *E. bulbosa*, Antioxidant activity, Anticancer activity, Photocatalysis.

INTRODUCTION

In recent years, nanotechnology has experienced remarkable growth in both development and application, emerging as a transformative force across various scientific domains [1]. As a multidisciplinary field, it plays a pivotal role in advancing technologies that improve the quality of human life. Within this expansive domain, green nanotechnology has garnered significant attention for its eco-friendly and cost-effective approach to nanoparticle synthesis, particularly through the use of plant extracts [2]. This method aligns with the principles of sustainable chemistry, offering a simpler, safer and more environmentally responsible alternative to conventional physical and chemical synthesis techniques [3-6]. A growing body of research has demonstrated the successful biosynthesis of various metal and metal oxide nanoparticles using botanical sources, enabling diverse applications across biomedical, environmental and industrial sectors [7-9]. Among these, zinc oxide nanoparticles (ZnO NPs) have emerged as especially promising due to their unique physicochemical properties. ZnO NPs are valued for their broad applicability in various fields, including energy storage, electronics, textiles, cosmetics, healthcare, sensors, semiconductors and catalysis [10]. More recently, ZnO NPs have gained recognition in agriculture, where they show potential for enhancing crop productivity and disease resistance [11,12]. Their biocompatibility and relatively low toxicity further distinguish them from other metal-based nanoparticles, making them a safer choice for biological and environmental applications [13,14]. Notably, their excellent photocatalytic activity enhances their effectiveness in processes such as wastewater treatment, underlining their versatility and significance in advancing sustainable technologies [15].

Eleutherine bulbosa, a medicinal bulb rich in bioactive phytochemicals such as phenolic compounds, flavonoids, alkaloids and terpenoids [16-18], has emerged as a promising candidate for the green synthesis of ZnO NPs. Owing to its well-documented antioxidant, antimicrobial and anticancer properties, *E. bulbosa* holds significant potential in both the food industry and biomedical sectors [16]. Notably, ZnO NPs are classified as "Generally Recognised as Safe" (GRAS) by the U.S. FDA [19], supporting their wide-ranging applications in biomedicine including antioxidant and antimicrobial therapies, wound healing, antidiabetic treatments, cancer therapeutics and targeted drug delivery systems [20-22]. The integration of such biogenic nanoparticles marks a forward-thinking approach to sustainable nanotechnology with broad societal benefits.

Maintaining a balance between free radicals and antioxidants is crucial for metabolic health, as excessive free radicals cause oxidative stress, contributing to diseases such as diabetes, inflammation and cancer. Natural antioxidants are increasingly studied due to concerns over synthetic alternatives [23,24]. In this work, aqueous bulb extract of *E. bulbosa* was used to synthesize ZnO NPs, with its phytochemicals acting as reducing, oxidizing, and capping agents. The nanoparticles were characterized using FT-IR, UV-Vis, XRD, SEM and HR-TEM. Antioxidant activity was tested *via* DPPH assay, cytotoxicity *via* MTT assay against MDA-MB-231 cells and photocatalytic performance through methylene blue degradation under UV light. This eco-friendly, low-cost approach uses readily available material, mild conditions and simple equipment, highlighting the potential of *E. bulbosa*-mediated ZnO NPs for biomedical and environmental applications.

EXPERIMENTAL

All chemicals, reagents and analytical-grade materials used in this study were procured from Sigma-Aldrich and used without further purification.

Extraction of plant material: Fresh bulbs of *Eleutherine bulbosa* were collected from Karivattom, India, with guidance from local inhabitants. The identity of plant material was verified by the Department of Botany, University of Kerala. The bulbs were washed three times with deionised water, air-dried and ground into a fine powder, which was stored in an airtight container for further use. Portions of the powder were extracted using chloroform, hexane, ethyl acetate, methanol and water for phytochemical analysis to confirm the secondary metabolites. For preparation, 6 g of powdered bulbs were mixed with 100 mL of deionised water, stirred and heated at 60 ºC for 1 h, cooled and filtered twice through Whatman No. 1 paper. The resulting extract was stored at 4 ºC for for further analysis [25].

Green synthesis of ZnO nanoparticles: Zinc acetate dihydrate ($Zn(CH_3COO)_2 \cdot 2H_2O$) was used as precursor for ZnO NPs synthesis, while sodium hydroxide (NaOH) served as the pH-modifying agent. Initially, 4 g of zinc acetate dissolved in 50 mL of deionised water was added to 10 mL of plant extract under continuous stirring. Subsequently, 1 M NaOH was added dropwise to adjust the pH to 8. The reaction mixture was again stirred and heated at 60 ºC for 2 h using a magnetic stirrer until a white precipitate formed, indicating the formation of ZnO NPs. The resulting precipitate was collected by centrifugation at 4000 rpm for 10 min and dried overnight in a hot air oven. Finally, the dried material was calcined in a muffle furnace at 400 ºC for 1 h. The obtained powder of ZnO NPs was stored for further characterisation and application studies.

Characterisation: The successful formation of ZnO NPs was confirmed through a series of advanced characterisation techniques. UV–Visible spectroscopy (Shimadzu UV-2450 spectrophotometer) was used to monitor the optical properties of the synthesised ZnO NPs. Fourier Transform Infrared Spectroscopy (FTIR) analysis was conducted in the range of 4000-400 cm^{-1} using the IR Prestige-21 (Shimadzu) *via* the KBr pellet method, identifying functional groups involved in the nanoparticle stabilisation. To evaluate the crystalline structure and estimate the average crystallite size, X-ray diffraction (XRD) analysis was carried out using Cu$K\alpha_1$ radiation at a scan rate of 1º/min. Thermogravimetric analysis (TGA) was conducted using a Perkin-Elmer TGA 4000 system to investigate the thermal stability and decomposition behaviour of the nanoparticles. The surface morphology and structural features were examined using scanning electron microscopy (SEM) on a TESCAN VEGA3 operated at 30 kV. Elemental composition was determined using energy dispersive X-ray spectroscopy (EDX), with a carbon-coated copper grid employed to prevent interference from elemental peaks. For detailed insights into particle size, shape and dispersion, high-resolution transmission electron microscopy (HRTEM) was carried out using a FEI Tecnai G2 F20 S-TWIN HR(S)TEM, operating at an accelerating voltage of 200 kV. The selected area electron diffraction (SAED) patterns were recorded to validate the crystalline nature of the ZnO NPs.

***In vitro* antioxidant activity:** The antioxidant potential of the synthesised ZnO nanoparticles was evaluated using the DPPH (2,2-diphenyl-1-picrylhydrazyl) free radical scavenging assay, following the method described by Safawo *et al*. [26] with minor modifications. A 3 mL aliquot of 100 μM DPPH solution, prepared in methanol, was mixed with 1 mL of ZnO NPs or plant extract solutions at varying concentrations (20, 40, 60, 80 and 100 μg/mL). The mixture was vigorously shaken using an orbital shaker and then incubated in a dark chamber at room temperature for 30 min to ensure complete reaction. The decrease in absorbance, indicative of DPPH radical scavenging, was measured at 517 nm using a UV-visible spectrophotometer. The percentage of radical scavenging activity (RSA) was calculated using the following formula:

$$\text{Radical scavenging activity (\%)} = \frac{A_c - A_s}{A_c} \times 100$$

where A_c and A_s are absorbances of the control and sample, respectively.

Cytotoxicity assay: Human triple-negative breast cancer cells (MDA-MB-231) were seeded at a density of 1×10^4 cells per well in 96-well plates using Dulbecco's Modified Eagle Medium (DMEM) supplemented with 10% fetal bovine serum (FBS) and 1× antibiotic-antimycotic solution. The cells were incubated at 37 ºC in a humidified atmosphere containing 5% CO_2 for 24 h to allow growth. Following incubation, the cells were gently washed with phosphate-buffered saline (PBS) and treated with varying concentrations of the test sample. Doxorubicin (IC_{50} = 3.8 μg/mL) was used as the positive control. Treatments were carried out in serum-free DMEM and incubated for an additional 24 h under the same conditions. After treatment, the medium was replaced with 0.5 mg/mL MTT solution prepared in PBS and the cells were incubated for 4 h at 37 ºC to allow for formazan crystal formation. Subsequently, the wells were washed with PBS and the MTT solution was discarded. The resulting formazan crystals were dissolved by adding 100 μL of DMSO to each well and mixed thoroughly. The formation of purple-blue formazan dye indicates mitochondrial metabolic activity, correlating with cell viability. The absorbance of the solubilised formazan was measured at 570 nm using a microplate reader [27].

Photocatalytic activity: The photocatalytic efficiency of ZnO NPs was evaluated using methylene blue (MB) dye as a model pollutant. A 10 ppm MB solution was prepared by dissolving it in 100 mL of deionised water. Subsequently, 0.1 g of ZnO NPs was added to the solution and the suspension was magnetically stirred in dark for 15 min to achieve adsorption–desorption equilibrium. Following this, the mixture was irradiated under UV light and aliquots were collected at 20 min intervals. The absorbance of each sample was measured using a UV-visible spectrophotometer to monitor dye degradation. The photocatalytic degradation efficiency was calculated using the equation:

$$\text{Dye removal (\%)} = \frac{A_o - A_t}{A_o} \times 100$$

where A_o is the initial absorbance of the dye solution and A_t is the absorbance at time t.

RESULTS AND DISCUSSION

UV-visible analysis: The UV-visible absorbance spectrum of the green-synthesised ZnO NPs exhibited a prominent absorption peak at 360 nm, as exhibited in Fig. 1. This blue-shifted absorption, typically observed within the range of 300-400 nm, is characteristic of ZnO NPs and confirms their successful formation [28]. The absorption peak at 360 nm corresponds to an optical band gap energy (E_g) of approximately 3.44 eV. It is well known that the optical band gap of ZnO NPs can vary depending on factors such as synthesis route, particle size and surface chemistry. The calculated band gap in this study aligns closely with the reported values for standard ZnO NPs, further validating the efficacy of the green synthesis approach.

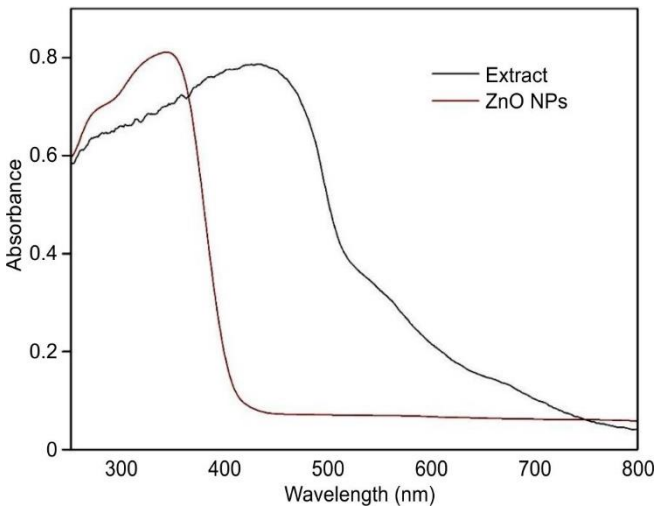

Fig. 1. UV-vis spectra of plant extract and synthesised ZnO NPs

The UV-visible spectral analysis further confirms the biosynthesis of ZnO NPs, as evidenced by the distinct absorption peak near 360 nm. The observed shift and narrowing of the peak compared to the plant extract support the formation of nanoscale ZnO with altered optical characteristics. The broad absorption of the plant extract highlights its role in nanoparticle formation through reduction and stabilisation mechanisms.

FT-IR studies: The FT-IR spectrum of the synthesised ZnO NPs, compared with the extract, as shown in Fig. 2, exhibits the characteristic absorption bands that confirm the formation and surface functionalities of ZnO NPs. Possible biomolecules responsible for the reduction of ZnO and the capping agent of bioreduced ZnO NPs through particular bond vibration peaks. The absorption bands at 3450, 2936, 2884, 1645, 1465, 1354, 1252, 953 cm^{-1} in the plant extract are shifted into 3430, 1589, 1346, 935, 522, 500, 488 cm^{-1} in the synthesised ZnO NPs. Most notably, a strong and well-defined absorption band between 600-500 cm^{-1} is attributed to Zn–O stretching vibrations, the spectrum confirms the successful formation of ZnO NPs. This shows that the peak sharpness indicates a high degree of purity [29,30]. The peak observed at 3430 cm^{-1} corresponds to O–H stretching indicating the hydroxyl group on the nanoparticle surface. These –OH groups likely originate from adsorbed moisture or residual phytochemicals derived from the plant extract used during green synthesis. These groups enhance photocatalytic efficiency by participating in ROS generation. The peak at 1589 cm^{-1} indicates H–O–H bending vibrations, corroborating the presence of adsorbed water molecules. The peak around 1550-1440 cm^{-1} showed the stretching of the N–H vibration [31], whereas peaks around 3000-2850 cm^{-1} represent aliphatic C–H stretching. The range of 1350-1200 cm^{-1} is for aromatic amines and 1250-1000 cm^{-1} is assigned to C–O stretching vibrations, typically found in alcohols, esters or ethers, reinforcing the presence of bio-organic compounds interacting with the ZnO surface or sometimes overlapping with C-N stretches. The region around 1460-1400 cm^{-1} is rich in C–H bending modes in various amino acids side chains in protein molecules and asymmetric stretching of carboxylate ions [32]. The bands from the analysis confirmed the amino acid residues of carbonyl groups and proteins have a stronger ability to bind metal ions and stabilize the formation of ZnO NPs in aqueous medium [31]. The non-appearance of organic peaks suggests minimal contamination, validating a clean synthesis process and ensuring high photocatalytic performance. The presence of Zn-O stretching and OH bending vibrations in the FT-IR spectrum serves as evidence for the successful synthesis of ZnO NPs.

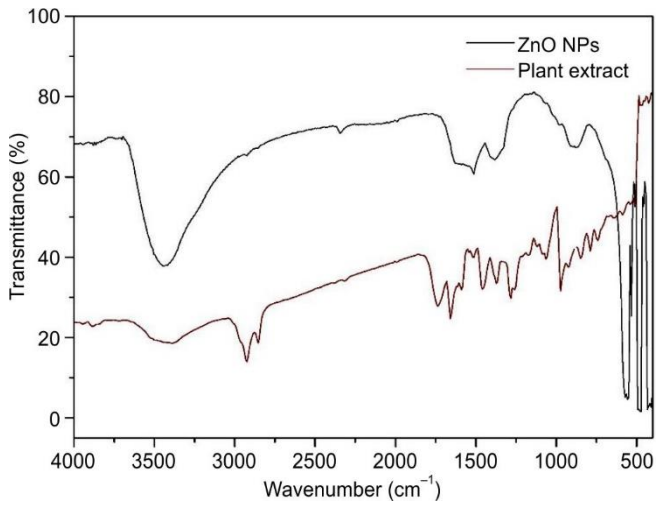

Fig. 2. FTIR spectra of plant extract and synthesised ZnO NPs

XRD analysis: The crystalline structure of the synthesised ZnO NPs was characterised using X-ray diffraction (XRD) and the corresponding diffraction pattern is shown in Fig. 3. The diffraction peaks observed at 2θ values of 31.45º, 34.12º, 36.2º, 47.22º, 56.34º, 62.60º, 66.14º, 67.62º, 68.76º and 76.61º correspond to the crystal planes (100), (002), (101), (102), (110), (103), (200), (112) and (201), respectively. These peaks align precisely with the standard diffraction data reported in the JCPDS card No. 036-1451, confirming the formation of a hexagonal wurtzite structure of ZnO. Among the peaks, the most intense reflections were noted at 36.2º, 31.45º and 34.12º, corresponding to the (101), (100) and (002) planes, respectively. The high intensity and sharpness of these peaks indicate excellent crystallinity and phase purity of ZnO NPs, with no evidence of impurity phases. The average crystallite size (D) of the ZnO nanoparticles was estimated using the Debye-Scherrer equation:

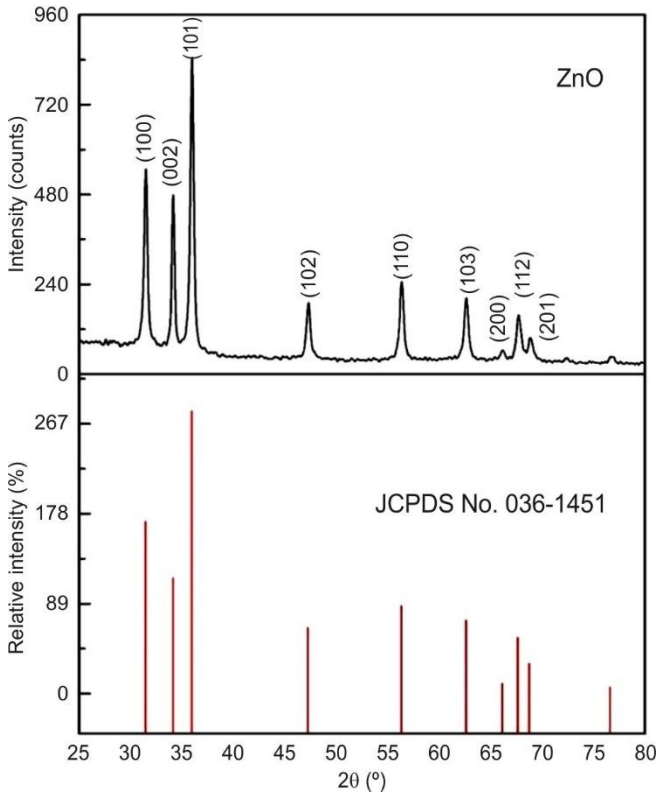

Fig. 3. XRD pattern of synthesised ZnO NPs

$$Dp = \frac{K\lambda}{\beta \cos\theta}$$

where D is the crystal size of ZnO NPs; K represents Scherrer's constant (0.9); λ is the wavelength of X-rays (1.541 Å); θ is the Bragg diffraction angle; and β is the full-width at half maximum (FWHM) of the diffraction peak corresponding to the plane (101).

Using this formula, the calculated average crystallite size of the ZnO NPs was found to be approximately 27.21 nm. This nanoscale dimension is consistent with the particle size observed in HR-TEM images, which reveal individual ZnO NPs composed of several closely packed nanocrystallites, further validating the formation of well-defined, crystalline ZnO nanostructures synthesised *via E. bulbosa* bulb extract.

Morphological studies: The surface morphology, elemental composition and crystalline structure of green synthesised ZnO NPs were thoroughly characterised using scanning electron microscopy (SEM), energy dispersive X-ray spectroscopy (EDX) and high-resolution transmission electron microscopy (HR-TEM), as presented in Figs. 4 and 5. SEM images (Fig. 4a-b) reveal that the ZnO NPs exhibit thin nanoflake-like structures with irregularly distributed spherical particles of varying sizes. The EDX spectrum (Fig. 4c) confirms the elemental composition, indicating the presence of only zinc (Zn) and oxygen (O), with strong characteristic peaks observed at 1.2 keV, 8.8 keV and 9.5 keV for Zn and a distinct peak at 0.6 keV for O, confirming the purity and successful formation of ZnO in its oxide state. HR-TEM analysis further supports the morphological observations, showing predominantly spherical particles with an average size in the range of 20-40 nm. The corresponding selected area electron diffraction (SAED) patterns (Fig. 5a-d) display well-defined diffraction rings, indicating the polycrystalline nature of the ZnO NPs. These results are in good agreement with the crystalline structure inferred from XRD analysis, thereby validating the successful synthesis of crystalline ZnO NPs *via* the green route.

Thermal studies: Thermogravimetric analysis (TGA) was conducted to evaluate the thermal stability, decomposition behaviour and residual content of the green-synthesised ZnO NPs. The analysis was carried out in a N_2 atmosphere with a heating rate of 10 ºC/min, ranging from 30 ºC to 950 ºC, using approximately 9 mg of sample. The resulting thermogram is illustrated in Fig. 6. An initial slight weight loss observed below 150 ºC is attributed to the evaporation of physically

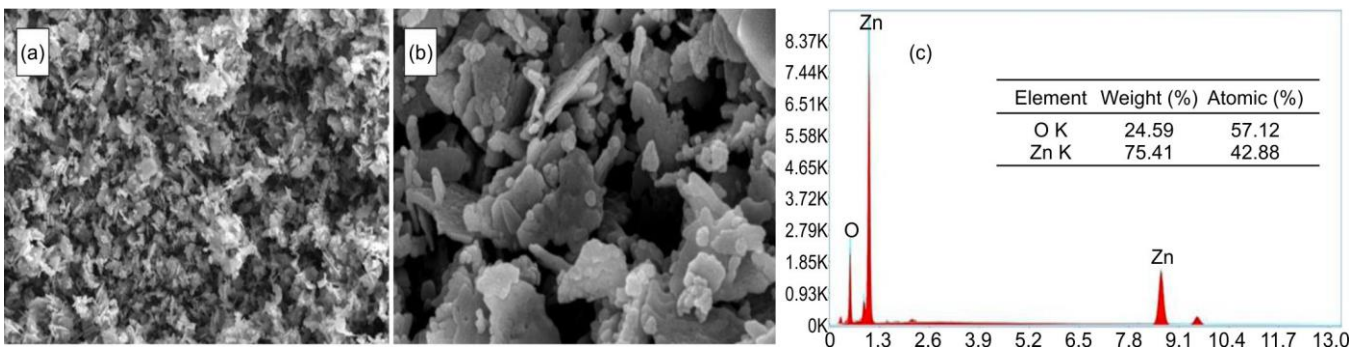

Fig. 4. (a,b) SEM micrographs and (c) EDX spectrograph of *E. bulbosa* mediated ZnO NPs

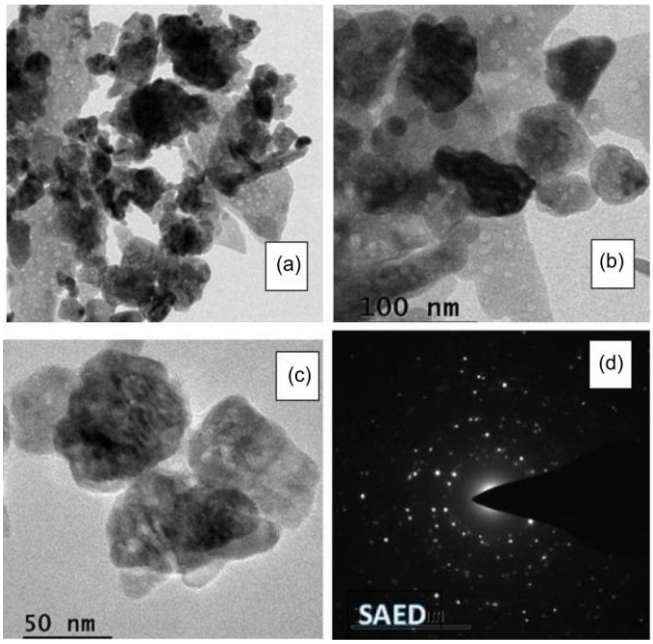

Fig. 5. (a-c) HR-TEM micrographs and (d) SAED pattern of *E. bulbosa* mediated ZnO NPs

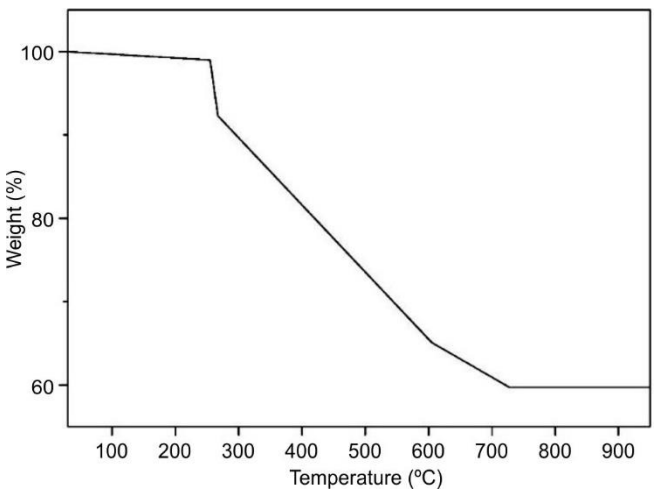

Fig. 6. Thermogram of *E. bulbosa* mediated ZnO NPs

adsorbed water and volatile phytochemical residues, indicating minimal surface-bound moisture [33]. Between 300 ºC and 600 ºC, a significant weight reduction occurs, decreasing from approximately 96% to 65%. This sharp decrease corresponds to the decomposition and burnout of organic constituents derived from the plant extract used in the process.

Beyond 600 ºC, the weight stabilizes, with a final plateau reached at around 59%, indicating the presence of thermally stable inorganic content, primarily ZnO. This implies that the peak decomposition of the char yield occurs at 720 ºC and the temperatures correspond to various percentages of weight loss. The minimal change in weight between 600 ºC and 900 ºC suggests that the organic matter has completely decomposed and a stable ZnO crystalline structure has formed. The observed thermal behaviour is consistent with previous reports on plant-mediated ZnO NPs synthesis, further confirming the removal of organic moieties and the thermal resilience of the ZnO core [34].

Comparative studies: The green synthesis of ZnO NPs using plant extracts has emerged as a sustainable approach; however, considerable disparities persist among the reported studies regarding nanoparticle size, shape, stability and functional effectiveness. These differences are mainly due to the biochemical makeup of the plant extract used. Table-1 presents a comparative overview of the key parameters between the present study and other selected green synthesis reports.

TABLE-1
COMPARATIVE ANALYSIS OF PHYSICO-CHEMICAL CHARACTERISATION OF ZnO NPs SYNTHESISED USING DIFFERENT PLANT EXTRACTS

Plant	Crystallite size (nm)	Morphology	Ref.
Moringa oleifera	~30-40	Rod/spherical	[35]
Aloe vera	~35-50	Irregular/spherical	[36]
Azadirachta indica	~20-30	Spherical	[37]
Eleutherine bulbosa	27.21	Nanoflake/ spherical	Present study

Biological applications

Antioxidant activity: The biosynthesised ZnO NPs prepared from *E. bulbosa* bulb extract were evaluated for their antioxidant potential using the DPPH radical scavenging assay. Upon interaction with ZnO NPs, ascorbic acid (standard) and the plant extract, the characteristic deep violet colour of the DPPH solution gradually faded to pale yellow. This colour change signifies effective radical neutralisation and was further validated through a UV-visible spectrophotometer at 517 nm [38]. A dose-dependent increase in antioxidant activity was observed as the ZnO NPs concentration ranged from 20 to 100 µg/mL. Comparatively, the ZnO NPs exhibited superior radical scavenging activity over the plant extract, though slightly lower than that of the ascorbic acid standard at all tested concentrations, as illustrated in Fig. 7. The IC_{50} value (the concentration required to inhibit 50% of DPPH radicals) for ZnO NPs was determined to be 44.15 µg/mL, indicating potent antioxidant activity, while the plant extract exhibited a higher IC_{50} value of 60 µg/mL, reflecting comparatively lower efficacy.

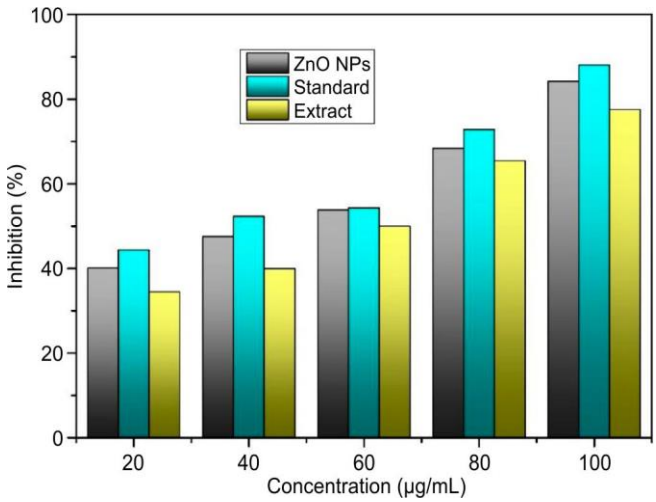

Fig. 7. Radical scavenging activity of plant extract and ZnO NPs

The relation between the antioxidant and photocatalytic activity lies in the material's ability to generate and quench reactive oxygen species (ROS). The dual behaviour demonstrates that ZnO NPs act both as ROS generators for environmental degradation under UV light and ROS scavengers, showing their biomedical potential even without light activation. So, the dual antioxidant and photocatalytic properties of ZnO NPs make them promising candidates for a range of applications, from protecting biological tissues against oxidative stress to degrading environmental pollutants.

Cytotoxic evaluation against breast cancer cells: The cytotoxic potential of green-synthesised ZnO NPs was gauged using the MTT assay against the human breast cancer cell line MDA-MB-231. Doxorubicin served as the positive control, while untreated cells were used as the negative control. Treatment with varying concentrations of ZnO NPs revealed a concentration-dependent cytotoxic response, significantly reducing cell viability compared to controls, as illustrated in Fig. 8. Notably, the IC_{50} value of ZnO NPs was calculated to be 21.12 ± 0.37 µg/mL, indicating potent anticancer activity. After 24 h of exposure, morphological changes such as cell shrinkage, rounding and loss of adherence were observed, suggestive of apoptosis or other cell death mechanisms induced by green-synthesised ZnO NPs. The IC_{50} value obtained for ZnO NPs highlights their efficacy in targeting cells while minimizing toxicity thresholds.

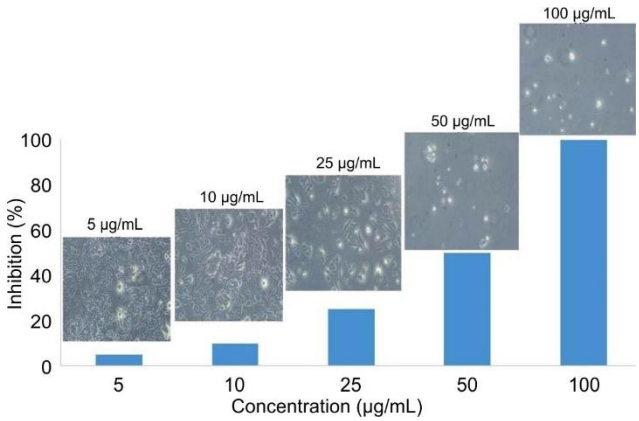

Fig. 8. Inhibition % of *E. bulbosa* mediated ZnO NPs against MDA-MB-231 cell lines

These findings underscore the dual role of green-synthesised ZnO NPs in exhibiting therapeutic efficacy while maintaining biocompatibility [39]. Their ability to selectively inhibit the proliferation of aggressive breast cancer cells positions them as promising candidates for future cancer therapies, particularly due to their sustainable synthesis route and favourable cytotoxic profile.

Photocatalytic activity: Initially, the methylene blue (MB) solution was stirred with ZnO NPs in the absence of light to distinguish the contribution of physical adsorption from photocatalytic activity. Minimal loss of dye concentration was observed, indicating negligible adsorption. The actual photocatalytic degradation was quantified by monitoring the reduction in absorbance at 665 nm over time, as presented in Fig. 9a. Upon UV exposure, a progressive decline in MB concentration was observed. Within the first 20 min, a degradation efficiency of 19.47% was recorded. The degradation rate increased with prolonged irradiation, reaching a maximum of approximately 80% after 100 min. At this point, the absorbance values approached zero, signifying near-complete decolourisation of the dye solution. The degradation was most rapid during the 20-40 min interval, as shown in Figs. 9b and 10. This phase likely corresponds to a surge in reactive oxygen species (ROS) generation, attributed to the catalytic activity of ZnO NPs under UV light [40]. The high availability of ROS, such as hydroxyl and superoxide radicals, accelerates the breakdown of dye molecules.

Initially, methylene blue molecules are adsorbed onto the surface of the ZnO NPs photocatalyst. Upon UV irradiation, ZnO NPs absorbs photons with energy equal to or greater than its band gap (hν), resulting in the excitation of electrons (e^-) from the valence band to the conduction band, leaving behind positively charged holes (h^+) in the valence band:

$$\text{ZnO NPs} + h\nu \rightarrow e^- + h^+ \quad (1)$$

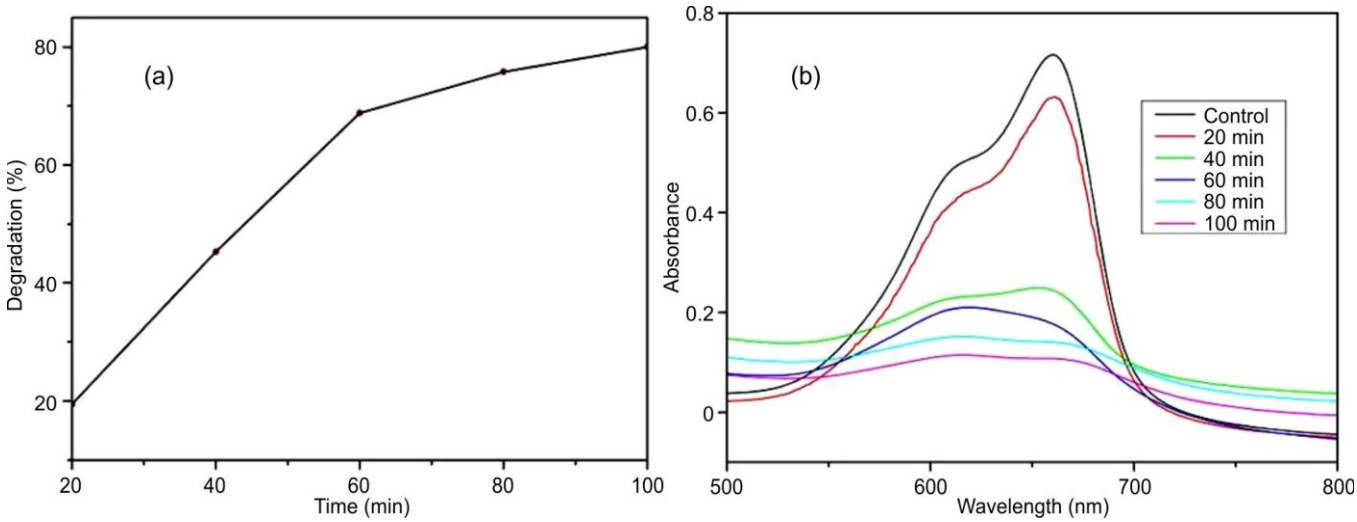

Fig. 9. (a) Photocatalytic % degradation of ZnO NPs, (b) UV-visible absorbance spectra of photocatalytic activity using methylene blue dye at different time intervals

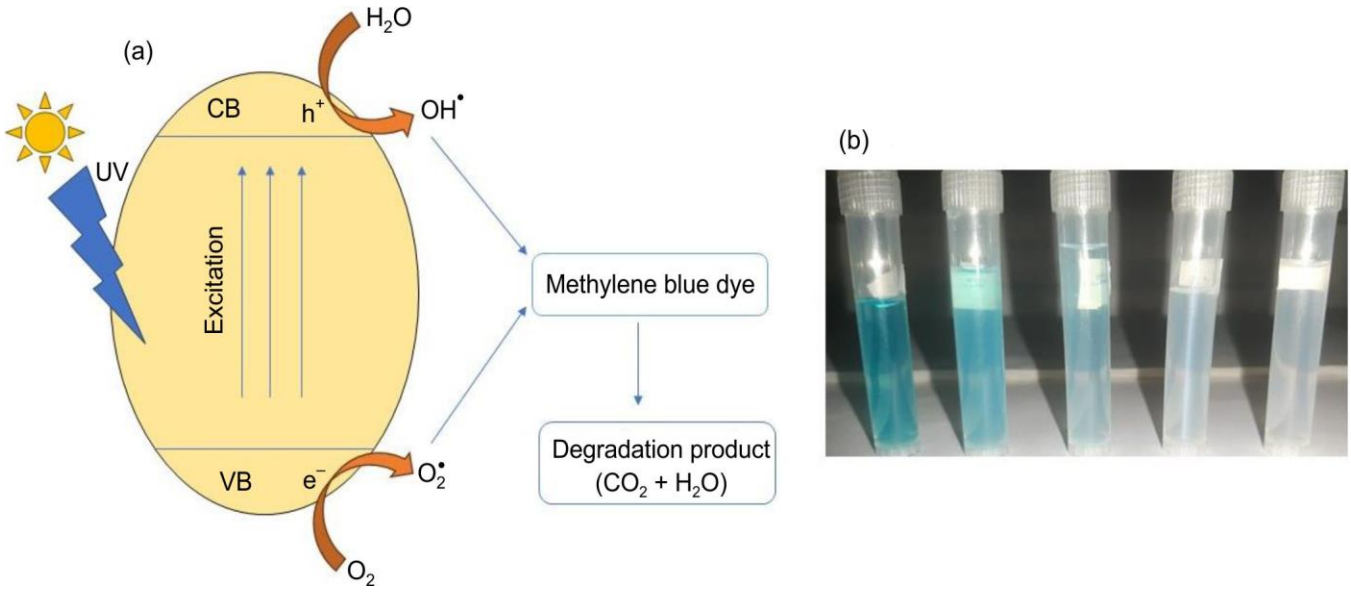

Fig. 10. (a) Schematic illustration of the photocatalytic degradation mechanism of methylene blue dye and (b) visual decolorisation of *E. bulbosa* mediated ZnO NPs

These photogenerated charge carriers initiate redox reactions on the catalyst's surface. The conduction band electrons reduce dissolved oxygen (O_2) to form superoxide radicals ($O_2^{\bullet-}$):

$$O_2 + e^- \rightarrow O_2^{\bullet-} \quad (2)$$

Simultaneously, valence band holes oxidize water (H_2O) or hydroxide ions to produce hydroxyl radicals ($^{\bullet}OH$):

$$H_2O + h^+ \rightarrow {}^{\bullet}OH + H^+ \quad (3)$$

Superoxide radicals can further react with protons to yield hydroperoxyl radicals ($HO_2^{\bullet}$):

$$O_2^{\bullet-} + H^+ \rightarrow HO_2^{\bullet} \quad (4)$$

These intermediates combine to form hydrogen peroxide (H_2O_2), which decomposes into additional hydroxyl radicals:

$$HO_2^{\bullet} + HO_2 \rightarrow H_2O_2 + O_2 \rightarrow 2OH^{\bullet} + O_2 \quad (5)$$

The highly reactive hydroxyl radicals generated during these reactions play a crucial role in attacking and decomposing dye molecules. They oxidize the complex dye structure into simpler, non-toxic end products such as carbon dioxide (CO_2) and water (H_2O):

$$^{\bullet}OH + Dye \rightarrow CO_2 + H_2O \text{ (Degradable products)}$$

The proposed photocatalytic degradation mechanism for methylene blue, as illustrated in Fig. 10a, demonstrates the interplay between photoexcitation, radical formation and dye mineralisation through oxidative and reductive pathways.

Comparative valuation and primacy of the present work with application: The ZnO nanoparticles synthesised in this work demonstrated pronounced anticancer efficacy, exhibiting an IC_{50} value of 21.12 µg/mL against MDA-MB-231 human breast cancer cells, which is notably lower than values reported for most plant-mediated ZnO nanoparticle systems. The superior cytotoxic response may be associated with the reduced particle size, distinctive hybrid morphology, and the synergistic contribution of bioactive phytochemicals adsorbed on the nanoparticle surface, which collectively enhance cellular interactions and oxidative stress-mediated damage. In parallel, the ZnO NPs showed remarkable photocatalytic efficiency, achieving approximately 80% degradation of methylene blue under UV irradiation within 100 min, outperforming many green-synthesised counterparts that typically report 60-75% degradation over longer irradiation periods. This enhanced photocatalytic behaviour is attributed to the enlarged effective surface area imparted by the hybrid morphology and the abundance of surface hydroxyl functionalities, which promote efficient reactive oxygen species generation. A comparative overview of the biological and photocatalytic performance parameters of the present study relative to previously reported green synthesis approaches is summarized in Table-2.

TABLE-2
COMPARATIVE ANALYSIS OF ANTICANCER AND PHOTOCATALYTIC ACTIVITY OF ZnO NPs SYNTHESISED USING DIFFERENT PLANT EXTRACTS

Plant	IC_{50} (MDA-MB-231, µg/mL)	Photocatalytic degradation of MB (%)	Ref.
Moringa oleifera	~25	~70% (120 min)	[35]
Aloe vera	>40	~65% (120 min)	[36]
Azadirachta indica	~30	~72% (120 min)	[37]
Typical green ZnO reports	30-50	60-75% in 120 min	
Eleutherine bulbosa	21.12	80% (100 min)	Present study

Cost-effectiveness and economic superiority of the present work: The synthesis strategy employed in this work offers clear economic advantages over several previously reported plant-mediated routes for ZnO NPs production. *E. bulbosa* bulbs are inexpensive, readily available across tropical and subtropical regions and require minimal preprocessing, which substantially lowers raw material and preparatory costs. By

TABLE-3
COST AND SUSTAINABILITY COMPARISON OF GREEN ZnO NPs SYNTHESIS METHODS

Synthesis route/ plant extract	Temperature & reaction time	Energy input & equipment needs	Solvent/ chemicals	Reported advantages	Ref.
Sea lavender (*Limonium pruinosum*)	Not specified, aqueous	Low-aqueous extraction	Water only	First report, low-cost, simple, but high IC_{50} (≈409 µg/mL)	[41]
Lotus leaf (*Nelumbo nucifera*)	Low-temperature solution combustion	Low-combustion method requiring minimal heat	Water extract	Facile, low cost, used in electronics (OFET)	[42]
General plant-mediated green synthesis	Variable	Reduced energy consumption, scalable	Water/bio-extracts only	Environmentally friendly, simple, time-efficient	[43]
Green *vs*. conventional synthesis	N/A	Reduced by ~30% energy use	Avoids toxic chemicals	Up to ~40% cost savings and ~50% higher throughput	[44]
Eleutherine bulbosa	60 ºC for 2 h; calcination at 400 ºC for 1 h	Low-standard hotplates and muffle furnace	Water only; no organic solvents	Eco-friendly, low-cost, scalable, multifunctional	Present study

contrast, several green synthesis approaches rely on seasonal or edible plant parts such as fruits, seeds, or flowers, which are often more expensive, compete with food resources or demand laborious extraction procedures involving multiple organic solvents. Significantly, the present method relies exclusively on deionised water as the extraction medium, completely eliminating the use of hazardous solvents. The synthesis proceeds under mild conditions, operating at a moderate temperature of 60 °C and ambient pressure, without the need for energy-intensive equipment such as autoclaves, microwave reactors or hydrothermal systems frequently employed in other green protocols. In addition, the relatively short reaction duration (2 h) and low calcination temperature (400 °C for 1 h) further reduce energy consumption while still yielding highly crystalline ZnO NPs with uniform nanoscale features. Taken together, these attributes establish the *E. bulbosa*-mediated approach as a cost-effective, energy-efficient, solvent-free, and scalable synthesis route. Its simplicity, affordability and multifunctional output position it favourably against many existing plant-based ZnO NP synthesis methods, particularly for large-scale and sustainable nanomaterial production. A comparative assessment of cost-effectiveness and sustainability parameters is provided in Table-3.

Conclusion

The green-synthesised ZnO nanoparticles (ZnO NPs) using the aqueous extract of *Eleutherine bulbosa* bulbs were confirmed through comprehensive characterization techniques. UV-Vis spectroscopy revealed a prominent absorption peak at 360 nm, indicating the formation of ZnO NPs. FTIR analysis confirmed the presence of characteristic Zn-O bond vibrations between 600-500 cm^{-1}, while XRD analysis revealed a crystalline wurtzite structure with an average crystallite size of 27.21 nm. SEM and HRTEM images further validated the hexagonal, flake-like morphology of the synthesised nanoparticles. Thermogravimetric analysis (TGA) demonstrated significant thermal degradation, with weight reduction from 96% to 65%, indicating high thermal sensitivity. The biosynthesised ZnO NPs exhibited notable antioxidant and anticancer activities, with IC_{50} values of 44.15 µg/mL and 21.12 µg/mL, respectively, underscoring their therapeutic potential. Furthermore, the ZnO NPs achieved an efficient 80% degradation of methylene blue, confirming their photocatalytic efficacy, outperforming most reported green syntheses.

ACKNOWLEDGEMENTS

The authors express their gratitude to The Standard Fireworks Rajaratnam College for Women, Sivakasi, India for supporting this research through a seed money project.

CONFLICT OF INTEREST

The authors declare that there is no conflict of interests regarding the publication of this article.

DECLARATION OF AI-ASSISTED TECHNOLOGIES

During the preparation of this manuscript, the authors used an AI-assisted tool(s) to improve the language. The authors reviewed and edited the content and take full responsibility for the published work.

REFERENCES

1. V. Aliko, L. Vasjari, E.S. Istifli, G. Gjonaj, F. Impellitteri, C. Faggio, E. Benedetti, S. Zugaro, A. Iannetta and M. Perugini, *Aquat. Toxicol.*, **276**, 107112 (2024); https://doi.org/10.1016/j.aquatox.2024.107112
2. M. Alam, *Nanotechnol. Rev.*, **10**, 1079 (2021); https://doi.org/10.1515/ntrev-2021-0069
3. K.V. Dhandapani, D. Anbumani, A.D. Gandhi, P. Annamalai, B.S. Muthuvenkatachalam, P. Kavitha and B. Ranganathan, *Biocatal. Agric. Biotechnol.*, **24**, 101517 (2020); https://doi.org/10.1016/j.bcab.2020.101517
4. R. Singh, C. Hano, G. Nath and B. Sharma, *Biomolecules*, **11**, 299 (2021); https://doi.org/10.3390/biom11020299
5. S. Wu, S. Rajeshkumar, M. Madasamy and V. Mahendran, *Artif. Cells Nanomed. Biotechnol.*, **48**, 1153 (2020); https://doi.org/10.1080/21691401.2020.1817053
6. C.G. Joshi, A. Danagoudar, J. Poyya, A.K. Kudva and B.L. Dhananjaya, *Process Biochem.*, **63**, 137 (2017); https://doi.org/10.1016/j.procbio.2017.09.008
7. A. Rana, S. Pathak, D.K. Lim, S.K. Kim, R. Srivastava, S.N. Sharma and R. Verma, *ACS Appl. Nano Mater.*, **6**, 8106 (2023); https://doi.org/10.1021/acsanm.3c01351
8. I. Ahmed, F.A. Mir and J.A. Banday, *BioNanoSci.*, **13**, 1541 (2023); https://doi.org/10.1007/s12668-023-01194-y
9. L. Devi, P. Kushwaha, T.M. Ansari, A. Kumar and A. Rao, *Biol. Trace Elem. Res.*, **202**, 3383 (2024); https://doi.org/10.1007/s12011-023-03920-9
10. K. Fatima, M. Asif, U. Farooq, S.J. Gilani, M.N. Bin Jumah and M.M. Ahmed, *ACS Omega*, **9**, 15882 (2024); https://doi.org/10.1021/acsomega.3c08143

11. S. Sabir, M. Arshad and S.K. Chaudhari, *Scient. World J.*, **2014**, 925494 (2014); https://doi.org/10.1155/2014/925494
12. M.A. Alghuthaymi, H. Almoammar, M. Rai, E. Said-Galiev and K.A. Abd-Elsalam, *Biotechnol. Biotechnol. Equip.*, **29**, 221 (2015); https://doi.org/10.1080/13102818.2015.1008194
13. C.A. Fernandes, N. Jesudoss M, A. Nizam, S.B.N. Krishna and V.V. Lakshmaiah, *ACS Omega*, **8**, 39315 (2023); https://doi.org/10.1021/acsomega.3c04857
14. S. Maher, B. Zamina, M. Riaz, S. Riaz, N. Khalid, M. Imran, S. Fahmid, H. Ishtiaq and S. Parveen, *ACS Omega*, **8**, 46715 (2023); https://doi.org/10.1021/acsomega.3c05947
15. Y. Sun, W. Zhang, Q. Li, H. Liu and X. Wang, *Adv. Sens. Energy Mater.*, **2**, 100069 (2023); https://doi.org/10.1016/j.asems.2023.100069
16. A.A. Kamarudin, N.H. Sayuti, N. Saad, N.A.A. Razak and N.M. Esa, *Int. J. Mol. Sci.*, **22**, 6747 (2021); https://doi.org/10.3390/ijms22136747
17. R.M.G. da Silva, C.P. Alves, F.C. Barbosa, H.H. Santos, K.M. Adão, F.O. Granero, C.C.M. Figueiredo, N. Nicolau Jr. and L.P. Silva, *J. Ethnopharmacol.*, **318**, 117005 (2024); https://doi.org/10.1016/j.jep.2023.117005
18. N. Panyachariwat, A. Jimtaisong and N. Saewan, *Cosmetics*, **11**, 111 (2024); https://doi.org/10.3390/cosmetics11040111
19. L. Motelica, B.S. Vasile, A. Ficai, A.V. Surdu, D. Ficai, O.C. Oprea, E. Andronescu, G. Mustatea, E.L. Ungureanu and A.A. Dobre, *Pharmaceutics*, **15**, 2470 (2023); https://doi.org/10.3390/pharmaceutics15102470
20. A. Anjum, M. Hashim, S.A. Malik, M. Khan, J.M. Lorenzo, B.H. Abbasi and C. Hano, *Cancers*, **13**, 4570 (2021); https://doi.org/10.3390/cancers13184570
21. S. Jha, R. Rani and S. Singh, *J. Inorg. Organomet. Polym.*, **33**, 1437 (2023); https://doi.org/10.1007/s10904-023-02550-x
22. M.A. Saifi, A. Negi, A. Kaur, Lakshya, R. Merugu, S. Negi and M.T. Yassin, *Inorg. Chem. Commun.*, **186**, 116214 (2026); https://doi.org/10.1016/j.inoche.2026.116214
23. L.A. Pham-Huy, H. He and C. Pham-Huyc, *Int. J. Biomed. Sci.*, **4**, 89 (2008); https://doi.org/10.59566/IJBS.2008.4089
24. G. Pizzino, N. Irrera, M. Cucinotta, G. Pallio, F. Mannino, V. Arcoraci, F. Squadrito, D. Altavilla and A. Bitto, *Oxid. Med. Cell. Longev.*, **2017**, 8416763 (2017); https://doi.org/10.1155/2017/8416763
25. V.S. Rani, *World J. Pharm. Res.*, **7**, 1022 (2018).
26. T. Safawo, B.V. Sandeep, S. Pola and A. Tadesse, *OpenNano*, **3**, 56 (2018); https://doi.org/10.1016/j.onano.2018.08.001
27. L. Florento, R. Matias, E. Tuano, K. Santiago, F. Cruz and A. Tuazon, *Int. J. Biomed. Sci.*, **8**, 76 (2012); https://doi.org/10.59566/IJBS.2012.8076
28. P. Jamdagni, P. Khatri and J.S. Rana, *J. King Saud Univ. Sci.*, **30**, 168 (2018); https://doi.org/10.1016/j.jksus.2016.10.002
29. G. Sangeetha, S. Rajeshwari and R. Venckatesh, *Mater. Res. Bull.*, **46**, 2560 (2011); https://doi.org/10.1016/j.materresbull.2011.07.046
30. S.J. Jun, S. Kim and J.H. Han, *J. Kor. Ceram. Soc.*, **35**, 209 (1998).
31. M. Ramesh, M. Anbuvannan and G. Viruthagiri, *Spectrochim. Acta A Mol. Biomol. Spectrosc.*, **136**, 864 (2015); https://doi.org/10.1016/j.saa.2014.09.105
32. S.K. Das, A.R. Das and A.K. Guha, *Langmuir*, **25**, 8192 (2009); https://doi.org/10.1021/la900585p
33. N.M. Nurazzi, M.R.M. Asyraf, M. Rayung, M.N.F. Norrrahim, S.S. Shazleen, M.S.A. Rani, A.R. Shafi, H.A. Aisyah, M.H.M. Radzi, F.A. Sabaruddin, R.A. Ilyas, E.S. Zainudin and K. Abdan, *Polymers*, **13**, 2710 (2021); https://doi.org/10.3390/polym13162710
34. B. Naiel, M. Fawzy, A.E.D. Mahmoud and M.W.A. Halmy, *Sci. Rep.*, **14**, 13459 (2024); https://doi.org/10.1038/s41598-024-63459-0
35. K. Sarwar, Z.-H. Nazli, H. Munir, M. Aslam and A. Khalofah, *Sci. Rep.*, **15**, 20413 (2025); https://doi.org/10.1038/s41598-025-08839-w
36. M. Manikanika and L. Chopra, *Mater. Today Proc.*, **72**, 1613 (2023); https://doi.org/10.1016/j.matpr.2022.09.413
37. N.O. Sanjeev, A.E. Valsan, S. Zachariah and S.T. Vasu, *J. Hazard. Toxic Radioact. Waste*, **27**, 04023027 (2023); https://doi.org/10.1061/JHTRBP.HZENG-1217
38. M. Naseer, U. Aslam, B. Khalid and B. Chen, *Sci. Rep.*, **10**, 9055 (2020); https://doi.org/10.1038/s41598-020-65949-3
39. S.S. Naser, B. Ghosh, F.Z. Simnani, D. Singh, A. Choudhury, A. Nandi, A. Sinha, E. Jha, P.K. Panda, M. Suar and S.K. Verma, *J. Nanotheranostics*, **4**, 248 (2023); https://doi.org/10.3390/jnt4030012
40. J. Gupta, J. Mohapatra and D. Bahadur, *Dalton Trans.*, **46**, 685 (2017); https://doi.org/10.1039/C6DT03713E
41. B. Naiel, M. Fawzy, M.W.A. Halmy and A.E.D. Mahmoud, *Sci. Rep.*, **12**, 20370 (2022); https://doi.org/10.1038/s41598-022-24805-2
42. A. Narayana, S.A. Bhat, A. Fathima, S.V. Lokesh, S.G. Surya and C.V. Yelamaggad, *RSC Adv.*, **10**, 13532 (2020); https://doi.org/10.1039/D0RA00478B
43. D. Mutukwa, R. Taziwa and L.E. Khotseng, *Nanomaterials*, **12**, 3456 (2022); https://doi.org/10.3390/nano12193456
44. A.I. Osman, Y. Zhang, M. Farghali, A.K. Rashwan, A.S. Eltaweil, E.M. Abd El-Monaem, I.M.A. Mohamed, M.M. Badr, I. Ihara, D.W. Rooney and P.-S. Yap, *Environ. Chem. Lett.*, **22**, 841 (2024); https://doi.org/10.1007/s10311-023-01682-3